Structures 67 (2024) 106987

Contents lists available at ScienceDirect

Structures

journal homepage: www.elsevier.com/locate/structures

Lateral response of post-tensioned pendulum shear walls

P.F. Silva [a,*], C. Lagler [a], R. Burgueño [b]

[a] George Washington University, USA
[b] Stony Brook University, Rigoberto, USA

ARTICLE INFO

Keywords:
Earthquake engineering
Energy dissipation
Unbonded post-tensioned shear walls
Pendulum motion
Lateral response

ABSTRACT

This paper presents an experimental evaluation of a new interface configuration for unbonded post-tensioned shear (UPTS) walls. In the proposed configuration, the wall-base interface is shaped in a circular profile. This circular profile presents a major difference from the currently used flat profile at the wall-base interface of rocking UPTS walls. During lateral response, this circular profile induces the wall to predominantly rotate as a rigid body about a fixed point without uplift, and the system dissipates energy through the contact friction that develops at the wall-base interface. This rigid body motion resembles that of a pendulum, thereby designating this system as a *pendulum UPTS* wall. At this stage, research has demonstrated the many advantages of this system by proof-of-concept testing of a pendulum light-frame wood (LiF) UPTS wall specimen under increasing levels of post-tensioning force. Compared with rocking UPTS walls, experimental results demonstrate that besides performing damage-free when subjected to high drift levels, the proof-of-concept *pendulum LiF-UPTS* wall offers the following promising outcomes: (1) insignificant to no wall uplift, (2) insignificant to no wall base shear sliding, (3) reduced stress concentrations at the wall toes because contact stresses are distributed along the wall-base interface over a larger region, (4) nearly constant post-tensioning forces under high drift levels, which limits post-tensioning losses due to yielding of prestressing bars or tendons, (5) increase in energy dissipation capacity of the system through friction, and (6) decrease in the damping reduction factor and thus, reduction in the lateral displacement and force demands in *pendulum LiF-UPTS* walls. These research outcomes are likely to translate positively to other shear wall types, namely reinforced concrete (RC) precast *pendulum UPTS* walls.

1. Introduction

Conventional design of shear walls in lateral force resisting systems (LFRS), is based on energy dissipation mechanisms that rely on damage accumulation in either regions of plastic action in reinforced concrete shear walls [24,50] or through racking of light frame wood shear walls [13,36,55]. For instance, in reinforced concrete shear (RCS) walls the primary mode of energy dissipation in plastic hinges is through damage accumulation by concrete spalling and yielding of the longitudinal reinforcement. In conventional light-frame wood shear walls, the primary mode of energy dissipation in wall racking occurs as a result of fasteners slip [53]. Previous research has clearly shown that these mechanisms of energy dissipation can negatively impact the serviceability of LFRS because of the associated resulting damage [6,13]. Furthermore, these modes of response do not fit within the societal needs of achieving immediate occupancy following an extreme seismic event, reducing economic losses [11,19,24]; or, moreover, they can adversely affect the resiliency of local economies in the post-recovery phase [19]. Consequently, response of the built infrastructure during past earthquakes has clearly demonstrated the need to investigate new construction systems that can remain mostly damage-free.

In the sense of traditional unbonded post-tensioned shear (UPTS) walls the primary mode of wall performance is by rocking of walls about its toes. These rocking UPTS walls have been developed and implemented in seismic design for dealing with the above noted issues and are intended to achieve immediate occupancy following a seismic event [2,3,8,53,23,25]. Following the Precast Seismic Structural Systems (PRESSS) project [41], research on rocking reinforced concrete (RC) precast UPTS walls received worldwide attention. Experimental results from the PRESSS project and many others demonstrated that these systems can achieve immediate occupancy and minimize economic losses following large earthquakes [6,7,53,41,43]. These positive outcomes promoted the use of rocking RC precast UPTS walls as viable LFRS in seismic design [2,3,20,37]. More recently Chalarca et al. [10] conducted a seismic evaluation of an archetype building with structural walls composed of precast concrete panels connected through shear

* Corresponding author.
E-mail addresses: silvap@gwu.edu (P.F. Silva), carmenlagler@gwu.edu (C. Lagler), Burgueno@stonybrook.edu (R. Burgueño).

https://doi.org/10.1016/j.istruc.2024.106987
Received 22 February 2024; Received in revised form 11 June 2024; Accepted 22 July 2024
Available online 31 July 2024
2352-0124/Published by Elsevier Ltd on behalf of Institution of Structural Engineers.

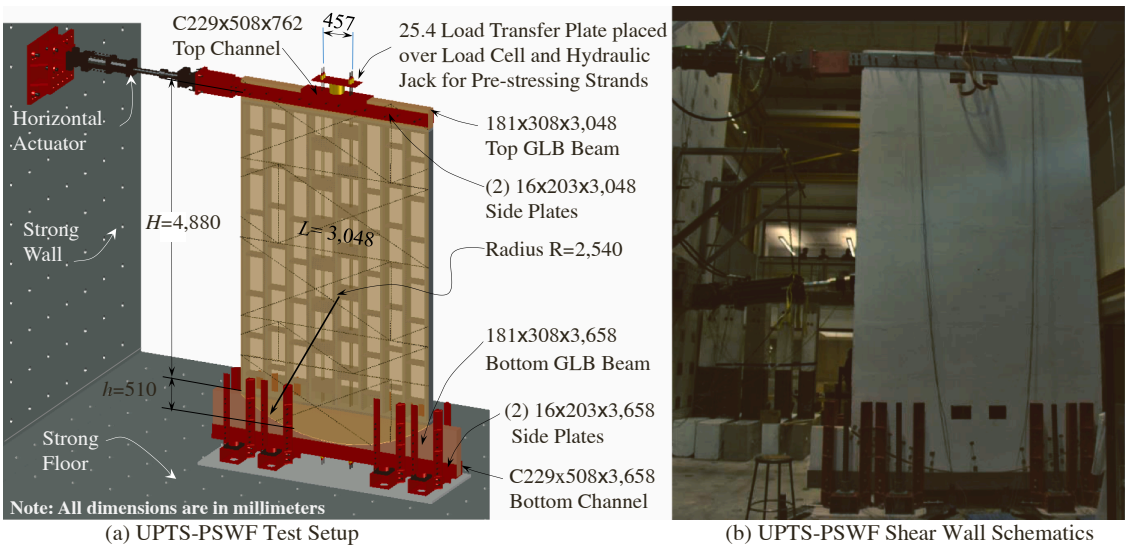

(a) UPTS-PSWF Test Setup (b) UPTS-PSWF Shear Wall Schematics

Fig. 1. UPTS-PSWF Shear Wall.

connectors and prestressed with unbounded steel bars using the FEMA P695 far-field ground motion. Results from their investigation demonstrated that UPTS walls are a viable LFRS in low-rise buildings [10].

The benefits of using rocking RC precast UPTS walls as LFRS derive from their damage-free and self-centering response under lateral loads [30,31,39,41,49,50]. The system's deformation capacity arises primarily from a decrease in the structural stiffness due to uplift and opening of the gap at the wall-base interface. With this response mechanism UPTS walls self-restore to a mostly damage-free configuration after a seismic event. However, the nonlinear response due to rocking lacks the energy dissipation capacity necessary to efficiently resist earthquakes [11,22,34], which poses some challenges if used directly in seismic design [35,38,43]. For instance, research has shown that compared to RCS walls, lack of energy dissipation in UPTS walls to seismic events results in greater lateral displacements and a higher number of displacement peaks [31,32,54]. Some additional challenges in using rocking RC precast UPTS wall as LFRS include concrete crushing at the wall toes, yielding of post-tensioning threaded bars or tendons, and wall shear sliding.

To enhance the performance of rocking RC precast UPTS walls, ACI ITG-5 [2,3] specifies diverse types of energy dissipation devices to be added. Of these, yielding connectors using a flexural mechanism have been identified as the most suitable for seismic design. To alleviate concrete crushing at the wall toes, ACI ITG-5.2 (R1.2.4.1) [3] indicates that confinement reinforcement in wall boundaries should be considered using displacement-based design concepts [3]. Another critical issue in rocking UPTS walls is the challenge of accurately estimating the level of compressive strains that these walls experience during rocking [27]. To deal with the uncertainty in proposing design compressive strains in the toe region, researchers have proposed replacing damaged toe regions with high performance fiber-reinforced concrete toe-blocks [12,27,52].

Regarding yielding of the post-tensioning threaded bars or tendons, ACI ITG-5.2 (5.6.1.1) [3] specifies drift limits intended to maintain the threaded bars or tendons within the elastic range as a means of preventing shear wall sliding and thus preserving the self-centering capabilities of UPTS walls [48]. In addition, ACI 318–19 [4] specifies that UPTS walls in regions of high seismic intensity must meet the design requirements of ACI ITG-5.1 [2] and ACI ITG-5.2 [3].

The system under current investigation represents a departure from commonly used rocking UPTS walls by featuring a circular profile at the wall-base interface. This interface geometry enables the wall to rotate predominantly as a rigid body about the center of the circular profile, and this motion is best characterized as an inverted pendulum without significant rocking or gap opening at the contact interface. To differentiate this motion from other UPTS rocking systems, this system has been designated as *pendulum UPTS* wall system.

The pendulum UPTS wall system shows great potential in mitigating the challenges facing rocking UPTS, whilst maintaining their damage-free capabilities. For instance, due to the curved interface geometry the potential for shear wall sliding is eliminated, thereby removing the need for placing sliding shear stoppers at the wall toes [6]. The system's kinematics show that a circular profile allows for higher relative displacements between coupled wall systems. This is relevant to the response of *pendulum UPTS* walls because it leads in an increase in the system's energy dissipation capacity in coupled walls with shear connectors. FEM results have also demonstrated that coupled *pendulum UPTS wall* systems have enhanced self-centering capabilities [47].

This paper presents the experimental evaluation of a *pendulum LiF-UPTS* wall concept under simulated lateral loads. In order to quantify the energy dissipation of this system, while performing damage-free when subjected to high drift levels, a single light-frame wood frame shear wall was tested multiple times under increasing levels of post-tensioning (PT) force. Three tests were conducted under varying post-tensioning force levels on the same wall unit, which could be reused since it remained undamaged. Experimental results demonstrated that the pendulum wall system was capable of gliding without separation along the base, remained undamaged, and dissipated considerable energy through contact friction. Test results also confirmed that the reduction in stress concentrations in the wall toe region eliminates the need for extra nailing requirements at the end of wood shear walls or the need for nail replacement after an earthquake [8]. In rocking RC-UPTS walls this response can also lead in reduction of confinement reinforcement in wall boundaries [3,6,35]. Test results further substantiate that at peak response, the energy dissipation capacity of the system was comparable to the amount of energy dissipation that develops from the hysteretic response of conventional RC walls [40], but significantly higher than what is feasible from LiF systems [8,53] or RC-precast rocking UPTS walls [6,31,32]. This is a valuable outcome, because energy dissipation capacity is an integral factor in decreasing the lateral displacement and force demands in the seismic design of LFRS [15,21,39].

2. Research significance

In order to achieve progress in UPTS wall technologies, the research herein addresses the following challenges: (1) compression stress

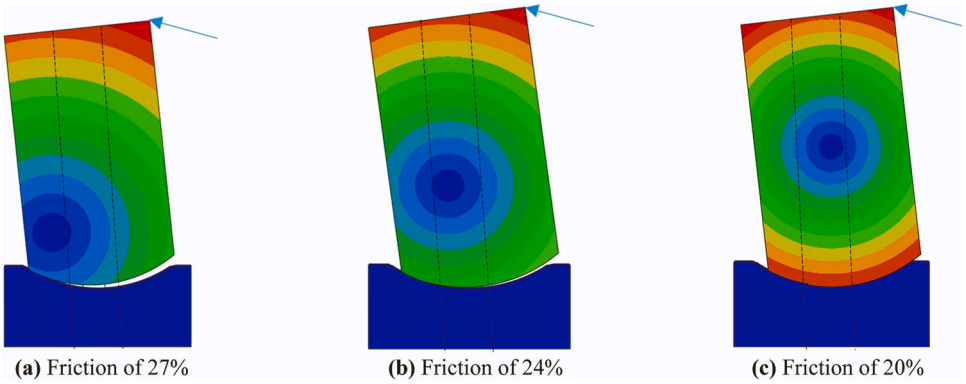

Fig. 2. FEM Simulations under Different Levels of Interface Friction.

concentration at wall toes, (2) yielding of the threaded bars or tendons, (3) wall shear sliding, and (4) design of a system that does not require design drift limits to maintain the many benefits of rocking UPTS systems. Although this paper focuses on a proof of concept for a light frame wood shear wall under increasing levels of post-tensioning force, computational simulations have also demonstrated that many of the promising results observed in this research program can be extrapolated to other systems such as *RC precast pendulum UPTS walls*. FEM results also demonstrated that the system's kinematics for a circular profile allows for higher relative displacements between coupled wall systems. This increases the energy dissipation capacity and the self-centering capabilities of coupled walls with shear connectors.

3. Experimental program

This section describes the experimental program conducted on an uncoupled pendulum light-frame wood (LiF) unbonded post-tensioned shear (UPTS) wall, which is designated herein as *pendulum LiF-UPTS* wall. The wall remained undamaged, which allowed performing multiple tests on this single wall. Although this paper focuses on three tests, other tests such as system calibration were performed but are not presented herein for brevity.

3.1. Test setup

The experimental program was conducted at The George Washington University (GWU) structural engineering research laboratory using the test setup presented in Fig. 1(a). The effective wall height H, defined as the distance from the top of the base block to the line of action of the lateral force, was 4880-mm, and the wall length, L, was 3048-mm. The wall was constructed with nominal 51 × 203-mm wood studs, which had an actual size of 38 × 181-mm. Shear resistance was increased by placing 19-mm plywood sheathing on both sides of the studs, which led to an overall wall thickness, t, of 219-mm.

Design of the test specimens was evaluated based on a parametric finite element analysis (FEA). The parametric FEA investigation was undertaken to investigate the influence of the following parameters on the response of pendulum *LiF-UPS* walls under lateral loads: wall aspect ratio, base radius, base friction, number and position of tendons, and initial posttensioning stress. Since this paper focuses mainly on the experimental program and test results, the parametric FEA are not presented for brevity.

The wall dimensions lead to a height-to-length (H/L) aspect ratio of 1.6, a length-to-thickness (L/t) ratio of 13.9, and a height-to-thickness (H/t) slenderness ratio of 22.3. Given the H/L aspect ratio and the point of load application, the wall was expected to respond with negligible shear deformations [5]. Furthermore, based on its H/t ratio the wall was classified as slender. However, it was well below the maximum permissible H/t of 50 by the American Wood Council [5].

Referring to Fig. 1(a), the base radius (R) was 2540-mm, which corresponds to an R/L ratio of 0.83. It is important to note that a wall with a R/L ratio of 0.5 corresponds to a wall interface in the shape of a perfect semicircle. As shown in Fig. 1(a), four unbonded 15 mm threaded steel bars were used in applying the post-tensioning (PT) force. In the longitudinal (L) and transverse (t) wall directions the spacing between the bars was 457-mm and 76.2-mm, respectively. These four threaded bars were fastened to the wall at the top and base against C299×508 mm steel channels. Further details regarding the construction sequence of the *pendulum LiF-UPTS* wall are presented in Section 3.3.

3.2. Test matrix

A single *pendulum LiF-UPTS* wall test unit, depicted in Fig. 1, was tested multiple times under the following increasing levels of PT force: 53-kN (12-kip), 107-kN (24-kip), and 133-kN (30-kip). These prestressing forces correspond to, respectively, 10 %, 20 %, and 24 % of the threaded bars allowable design force. The units were designated as *PT12P*, *PT24P* and *PT30P* where the PT load in kips was used in defining each test unit. For each PT level the test wall was subjected to fully reverse incremental cycling loading, details of which are discussed in Section 3.4. Since the *pendulum LiF-UPTS* wall remained undamaged it was feasible to perform multiple tests on this single wall.

At the onset of the research program, a series of 3D finite element analyses were performed using the ABAQUS software [1]. The finite element analyses (FEA) were performed considering the appropriate geometric dimensions, PT forces, and interaction conditions at the wall-base interface. Further details of the numerical analysis are published elsewhere [47,46] and are not elaborated herein for brevity.

One of the challenges encountered during the testing program was to ensure that the wall response was dominated by sliding at the wall-base interface with minimum to no uplift/rocking during any testing stage. To ensure the desired gliding response, FEA were conducted and results indicated that the response was mainly characterized by uplift/rocking response when the friction coefficient at the wall-base interface was above 24 %, as shown in Fig. 2(a) and (b).

Conversely, the pendulum response shown in Fig. 2(c) was achieved when a friction coefficient of 20 % or less was implemented in the 3D FEA model. For this friction coefficient the wall and base remain in full contact throughout the reversed cyclic loading protocol and the wall rotates predominantly as a rigid body about the center of the wall circular profile. In order to achieve the desired response and fiction coefficient, aluminum plates and friction reducing agents were investigated and finally applied at the wall-base interface to ensure a friction coefficient of less than 20 %. The friction reducing agent was a readily available off-the-shelf engine grease and had a reported viscosity grade of 99. This grease was applied along the entire length of the wall-base interface with a hand operated grease pump gun and spread by hand.

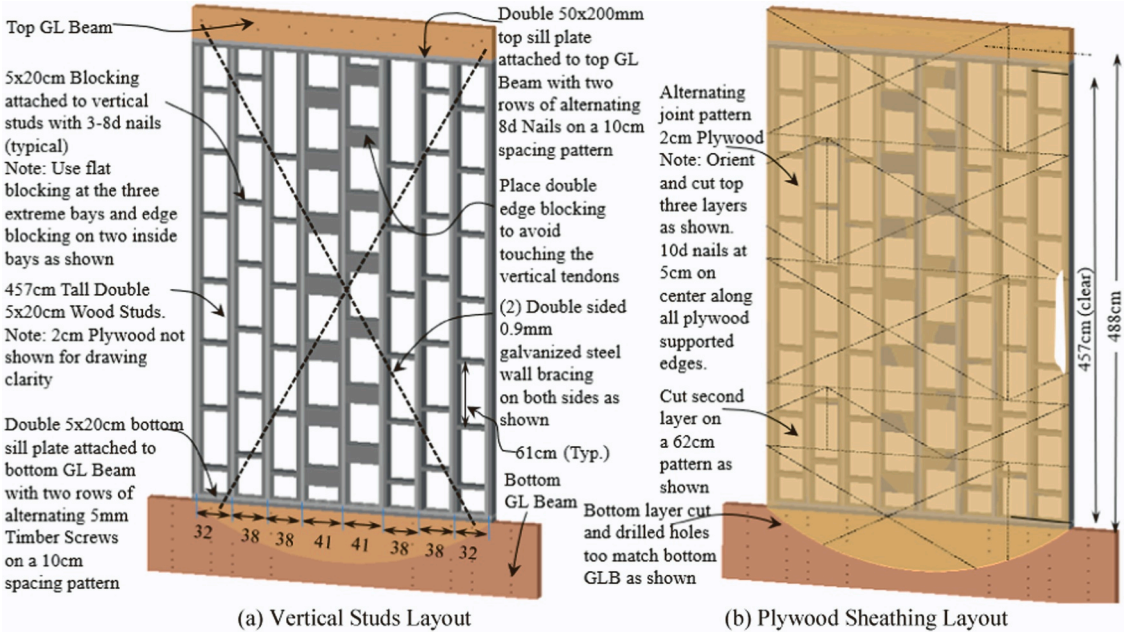

Fig. 3. UPTS-PSWF Shear Wall Construction.

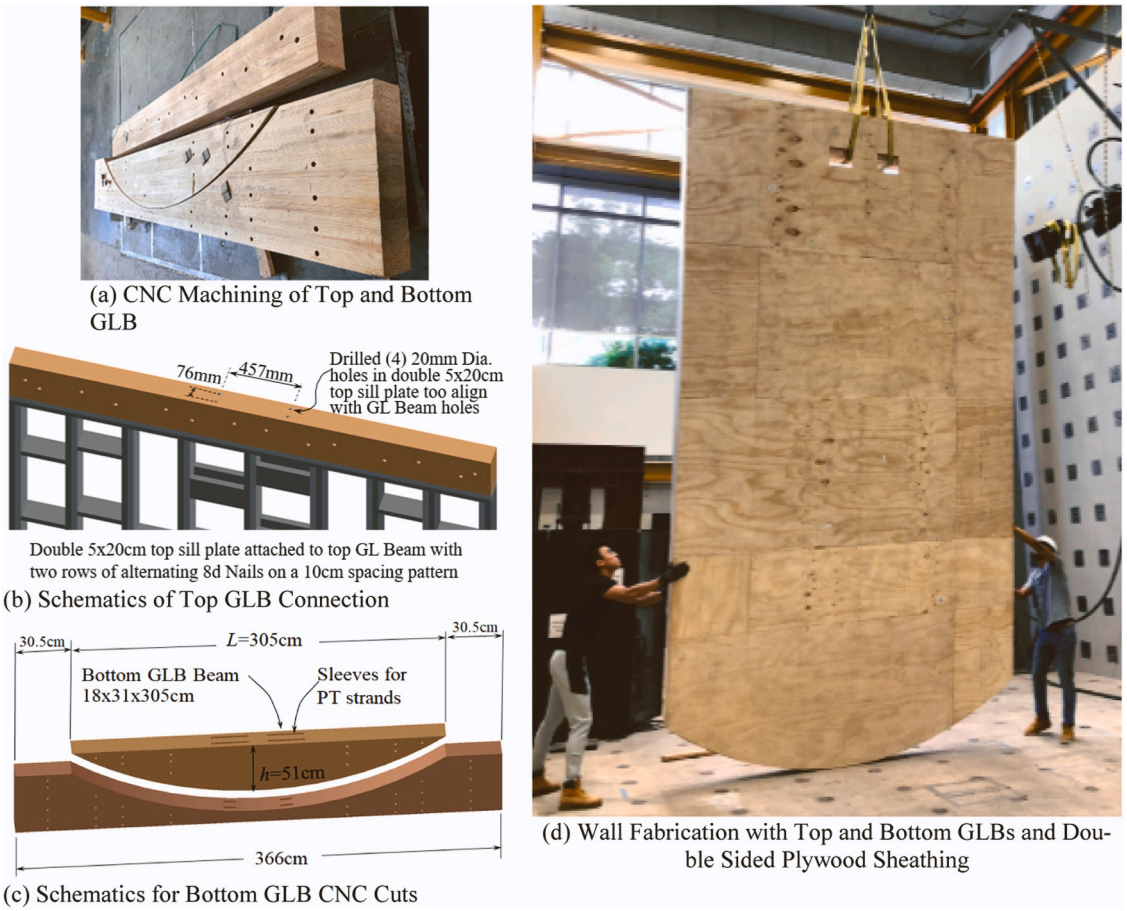

Fig. 4. Glulam Beam Installation on Wood Framing Wall.

Because of its high viscosity, this grease does not run when applied. In future research other types of materials employed in practice will also be investigated. These can include typical materials used in friction pendulum energy dissipation devices, such as: Polytetrafluoroethylene composites, ultra-high molecular weight polyethylene, and polyamide [17].

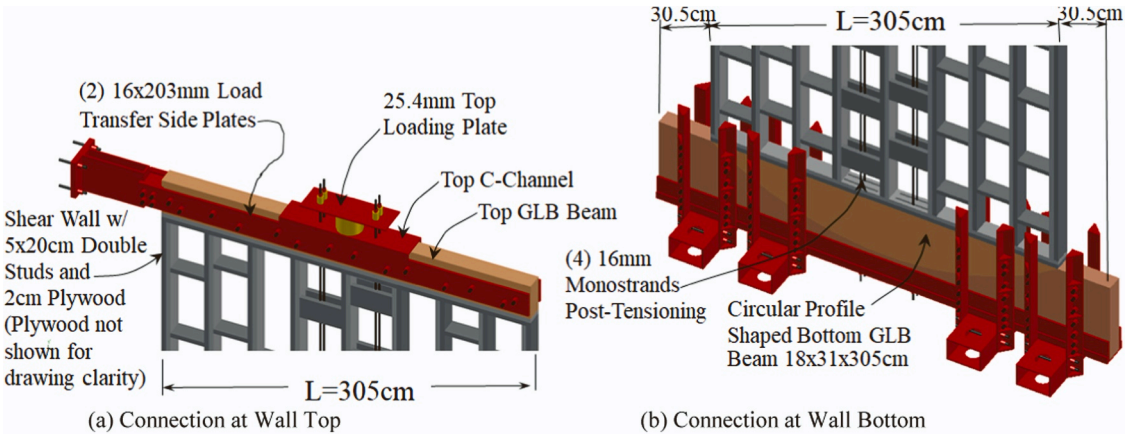

Fig. 5. Top and Bottom Wall Connections.

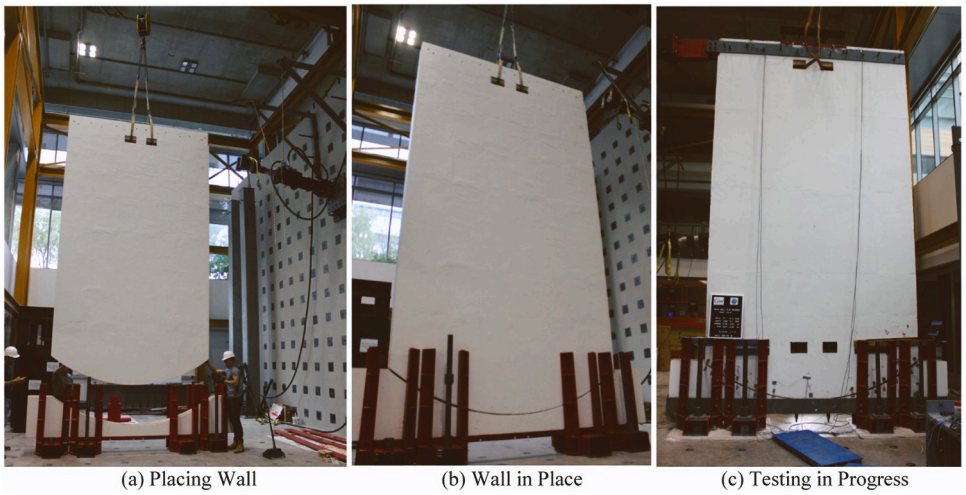

Fig. 6. Placing Wall over Base.

3.3. *Pendulum LiF-UPTS wall construction*

As shown in Fig. 3(a), the *pendulum LiF-UPTS* wall framing consisted of using nine sets of 457 cm long double nominal 5 × 20 cm wood studs, (exact size was 4 ×18 cm). In order to accommodate the relative motion between the wall studs and the internal threaded bars, the vertical wood studs were spaced symmetrically along the width of the wall at 32, 38, 38, and 41 cm.

Double 5 × 20 cm sill plates were nailed to top and bottom glulam beams (GLB) with two rows of 8d nails at 10 cm on center. The weak axis stability of the internal wood studs was increased by using double sided 2 cm × 122 cm x 244 cm plywood sheathing and 5 × 20 cm wood blocking according to the schematics outlined in Fig. 3(a). Plywood panels were placed on both sides according to the staggered pattern depicted in Fig. 3(b). The plywood nailing diagram consisted of 10d nails at a spacing of 5 cm along all blocked and supported edges. In addition, two diagonal 0.9 mm × 76 mm (20-gauge) wide galvanized steel braces were installed on either side of the wall as shown in Fig. 3 (a). This nailing diagram and plywood configuration provided a unit shear wall capacity of nearly 25 kN/m. The shear capacity was obtained using design tables from reference APA [51], which far exceeds the required unit shear demand of 15 kN/m. The required unit shear demand was based on an estimated shear force demand of 45 kN and a wall length of 3048 mm. This unit shear demand was obtained from FEA, and as previously stated results from the FEA are not presented herein for brevity.

As shown in Fig. 4(a), a series of 20 mm diameter holes were pre-drilled on the top and bottom GLBs. These pre-drilled holes were necessary to fasten steel plates to the wall and subsequently were used for the load transfer between the horizontal actuator and the wall, see Fig. 1(a). Schematics in Fig. 4(b) depict the connection of the top GLB to the wall.

As shown in Fig. 4(a and c), at the wall-base interface the circular shape was machine-cut from a single GLB and manufactured to the desired shape using CNC machining conducted offsite. Fig. 4(d) shows the construction stage immediately after the plywood sheathing was nailed to the top and bottom GLBs and the wall framing. Fig. 5(a) depicts details pertaining to the top loading plate for post-tensioning the threaded bars and the load transfer side plates for connection to the top GLB. Fig. 5(b) shows the wall base with vertical outriggers, which were provided as a means for controlling any potential out-of-plane deformation of the test unit. The final assembly of the wall is illustrated in Fig. 6(a) and (b), and Fig. 6(c) shows the wall test setup during testing in progress. As shown in Fig. 3(a) all the blocking in the center of the wall was placed sideways to avoid contact between the vertical tendons and the wall. Likewise, as shown in Fig. 4(c), CNC machine slotted holes were perforated in the GLBs to ensure that during lateral response the tendons did not compress against the GLBs, and therefore they were not subjected to shear stresses at the wall-base interface.

3.3.1. *Material properties*

The wood framing wall was constructed using Douglas-Fir Larch

Table 1
Summary of Relevant Static and Kinetic Coefficients of Friction (COF).

Surface Interaction [1]	Static COF, μ_S		Kinetic COF, μ_K	
	Mean (%) [5]	CV (%) [5]	Mean (%) [5]	CV (%) [5]
Dry GLB wood on Dry GLB wood[2]	72	6.21	52	13.81
Greased GLB wood on Greased GLB wood[2,3]	32	5.97	24	9.87
Dry aluminum on Dry aluminum[4]	62	6.41	42	12.60
Greased aluminum on Greased aluminum[3,4]	17	9.30	12	7.71

[1] All surfaces were polished with a circular sander using a 220-grit fine grade sand paper and cleaned with a brush.
[2] The wood surfaces were furnished by the glulam beam's manufacturer with the plane of the surface made at an angle with the laminations.
[3] Engine grease with a reported viscosity grade of 99 was used on all greased surfaces.
[4] Aluminum plates were cut to size and glued to the wood surfaces.
[5] The mean and the coefficient of variation (CV) were obtained from a minimum of five tests.

(DFL) Select Structural grade lumber studs. This lumber was chosen because of its dimensional stability, consistent material properties, and long-term durability. According to the manufacturer the specified design strength values for the shear parallel to grain, and compression parallel and perpendicular to the grain were, respectively, 1240 kPa, 4309 kPa, and 11,720 kPa. Compression strength perpendicular to the grain was especially relevant to ensure proper transfer of compression forces from the vertical wood studs to the top and bottom wood sill plates. The minimum modulus of elasticity was 4760 MPa.

The 20 mm plywood satisfied the APA Rated Sheathing standards and was produced as Structural I Sheathing [51]. This plywood provides enhanced racking and cross-panel strength properties for shear walls. As previously stated, the nailing diagram and plywood configuration provided a nominal unit shear wall capacity of nearly 25 kN/m.

The top and bottom top and bottom glulam beams (GLB) where DF 24 F-V4 with a modulus of elasticity of 11,720 MPa, and a nominal compression strength perpendicular to the grain of 5102 kPa.

The four 15 mm threaded steel bars used for posttensioning had a nominal minimum yield and ultimate strength of 157 kN and 191 kN, respectively. These values exceeded the maximum expected prestressing force, estimated at 80 kN per tendon.

3.3.2. *Coefficient of friction*

Calculated coefficients of static and kinetic friction for four different types of surfaces are reported in Table 1. It is important to note that the coefficients of friction (COF) were obtained via indirect methods, and using small sampling surfaces with a small wood block. As such, these COF values may be different those in the *pendulum LiF-UPTS* wall tests, which were conducted under high compressive loads. The COFs for the glulam beams in Table 1 are higher than those reported in the literature for wood surfaces because sliding is not occurring parallel to the grain. This is consistent with conclusions drawn from research projects on cross grain laminated veneer lumber [18]. COFs used in the numerical simulations was mainly to infer the limiting COF for which the wall behavior changes from uplift to pendulum motion. As such in the FEM model pendulum response is observed when the COF drops below 20 %. As shown in Table 1, values for greased aluminum surfaces were consistently below 20 %.

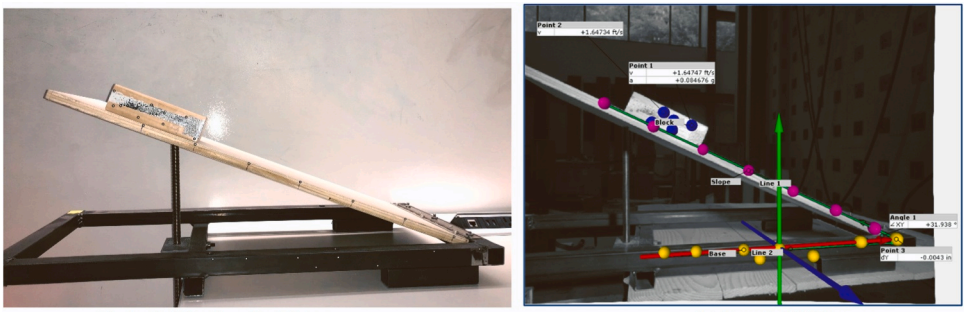

Fig. 7. Test Setup for Determining Static and Kinetic Coefficient of Friction.

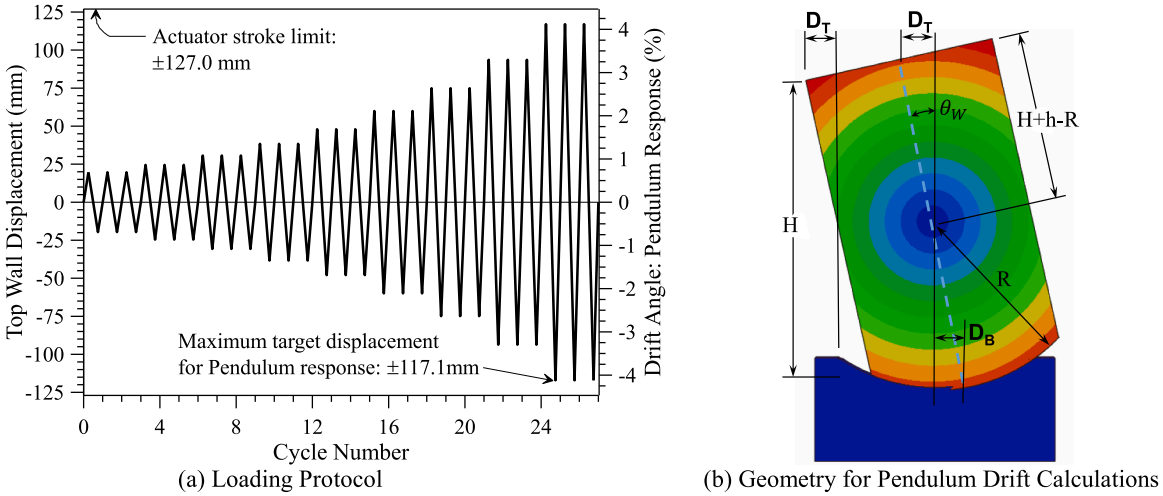

Fig. 8. Testing Protocol Based on ACI ITG-5.1 [2].

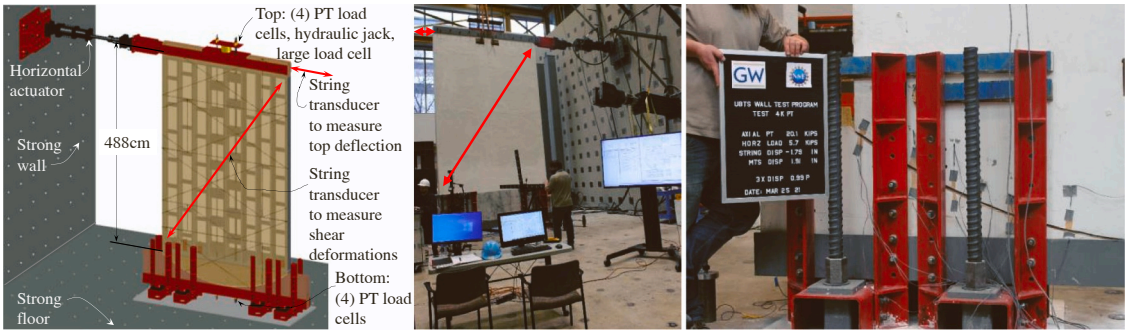

(a) Instrumentation Schematics (b) DIC and DAQ Systems (c) Strain Gages Installation

Fig. 9. Instrumentation used During Testing.

As shown in Fig. 7(a) the angled surface indirect test method was used to measure the static and kinetic coefficients of friction (COF) [42, 45]. The static COF, μ_S, was calculated as the angle required to impose initial motion on a wood block. The angle was measured using a Digital Image Correlation (DIC) system. The kinetic COF, μ_K, was determined by calculating the acceleration at seven tracking points placed on the wood block and along the inclined surface using Eq. (1). These tracking points are shown in the sample DIC image in Fig. 7(b).

$$\mu_K = \frac{a + g\sin(\theta)}{g\cos(\theta)} \tag{1}$$

In Eq. (1), a is the acceleration calculated by the DIC system at different tracking points, g is the gravitational acceleration, and θ is the angle of the inclined surface with respect to the horizontal. In all COF tests, digital images were recorded with a DIC system at a sampling rate of 100 frames/sec.

3.4. Testing protocol

After applying the initial post-tensioning (PT) force, testing progressed by subjecting the wall to three fully reversed cycles at each of the incremental displacement levels outlined in Fig. 8(a). This testing protocol followed the loading cycles provided in the research article by Brown et al. [8] and is in agreement with the established minimum experimental requirements stated in ACI ITG-5.1 [2]. Furthermore, this testing protocol is similar but not exactly to the same as the basic loading history suggested by CUREE for wood frame shear-wall testing [28]. The CUREE loading protocol was not followed, for a direct comparison to rocking UPTS walls, however the number of repeated loading cycles beyond 1 % drift in Fig. 8(a) were higher than according to the CUREE loading protocol.

ACI ITG-5.1 [2] stipulates that testing of UPTS walls shall be performed until at least failure of the system occurs or unless the system can achieve the following drift angles (in percent):

$$0.90\% \leq \quad \theta_W = 0.80 \quad (H/L) + 0.50 \quad \leq 3.00\% \tag{2}$$

Based on the height-to-width (H/L) aspect ratio of 1.6, the required drift level to establish an acceptance criterion for UPTS walls is 1.78 %, which results in the following relative top wall displacement:

$$\Delta_T = \theta_W H = 1.78\% \times 4,876.8 = 86.8mm \tag{3}$$

However, the target maximum displacement was increased to $\pm$ 117.1 mm or 4.12 %, which was within the stroke limit capacity of the actuator. These values are clearly higher than the required acceptance criteria values of 86.8 mm or 3 % drift ratio. This was implemented in order to evaluate if these walls can exceed the maximum stipulated drift level of 3 % without any significant level of damage. It can be shown that for systems responding primarily within a pendulum mode, the corresponding target pendulum drift angle is 4.12 % based on:

$$\theta_W = \frac{\Delta_T}{H + h - R} = \frac{117}{4,876.8 + 508 - 2,540}\% = 4.12 \quad \% > 1.78 \quad \% \tag{4}$$

In Eq. (3), H is the height of the wall, R is the base radius, and h is 508 mm. This deformation geometry is depicted in Fig. 8(b). It is important to emphasize that this research seeks to investigate systems characterized by a pendulum response without significant separation at the base interface, as depicted in Fig. 8(b). Furthermore, this proof of concept intends to show that the design of pendulum UPTS walls is not limited by drift levels necessary to maintain the many benefits of *pendulum UPTS* systems.

3.5. Instrumentation

Fig. 9 depicts the different instrumentation devices that were used during testing. The following is a list of instrumentation placed on the test unit and is used in this paper to present and discuss the response of each of the test units. Eight 223 kN low clearance load-washers (hollow core compression load cells) were placed between the threaded bars nuts and wall plates. Four of the load cells were placed at the connection of the threaded bars to the top of the wall and four were placed at the connection on the bottom of the wall. Placing load cells at each end of the threaded bars allowed for redundancy in data collection of the post-tensioning (PT) forces. Furthermore, during application of the PT force an additional large load cell was placed between the hydraulic jack and load transfer plate at the top of the wall. Fig. 9(a) also shows that one string displacement transducer was placed horizontally at the top of the wall to measure the wall top deflection, and one more string displacement transducer was placed along the diagonal direction to estimate shear deformations in the wall. A digital image correlation (DIC) system was employed for capturing images as depicted in Fig. 9(b), which were subsequently used to obtain localized full field displacements at the wall-base interface. Finally, Fig. 9(c) shows the installation of strain gages at the wall-base interface. Though only half of the wall is illustrated, the same strain gage layout was also used in the other half of the wall.

3.5.1. Data collection and synchronization

Data was collected and synchronized according to three patterns. First, data was collected and archived from the actuator control system (i.e., actuator load cell, displacement transducer and time) at a rate of 20 points per seconds resulting in 100,000 data points. Second, data was collected and archived from all the other instrumentation (except for the video camera and the DIC system) at a rate of one data point every 20 s leading to approximately 7000 data points per test. Finally, data was collected and archived from all instrumentation including the video camera and DIC system at a rate of one data point for every 2.54 mm (0.1 in.) increment in the wall top displacement. The video and DIC images were captured and synchronized with all the instrumentation

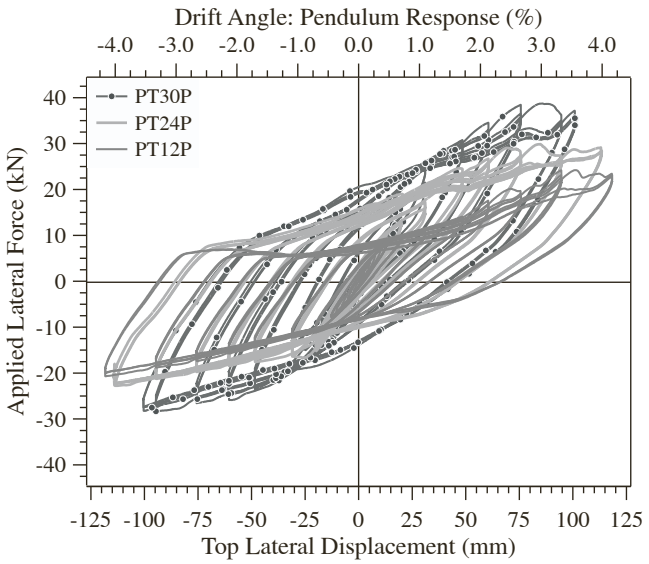

Fig. 10. Load-Deformation Response.

devices by the data acquisition system at the predefined displacement increments. This led to nearly 20–30 additional data points on average from each fully reversed loading cycle, leading to approximately 900 data points per test. This data collection pattern was necessary because of storage limitations of the DIC system, which can only store 950 images per test.

4. Experimental test results

4.1. Lateral load-deformation response

During each of the tests, the wall was subjected to 27 fully reversed displacement-controlled loading cycles according to the loading protocol shown in Fig. 8(a). Three tests were performed at increasing levels of post-tensioning (PT) force. Details on the applied PT force were previously discussed in Section 3.2. Fig. 10 depicts the actuator applied lateral force versus the wall top displacement and corresponding drift values. The load-deformation results depicted in Fig. 10 show substantial energy dissipation capacity of the system through contact friction.

Fig. 10 indicates that the three test units were capable of sustaining the applied reversed three cycles at the peak target displacement with stable hysteretic loops and no noteworthy losses in the lateral load between cycles at equal displacements. Based on the drift angles, the test units complied within the minimum experimental requirements of ACI ITG-5.1 [2], and clearly exceeded the required drift angle of 1.78 % by a significant amount at 4.16 %, 3.98 % and 3.55 % for each of the three tests, respectively. During each of the three tests and using test *PT12P* as the baseline unit, the peak lateral forces represent a successive increase of 18.8 % and 43.7 %, which indicates a noticeable effect of the PT force on the lateral load capacity.

As previously discussed, finite element analyses have shown that a reduction in the friction coefficient at the wall-base interface modifies the response of UPTS systems from an uplift mode to a pendulum mode, see Fig. 2. To reflect this desired response, relevant modifications consisted of placing aluminum plates coated with a high viscosity grease at the wall-base interface. The load-deformation response in Fig. 10 clearly indicates that the application of the interface materials was successful in achieving the desired response and energy dissipation capacity of the test units, which is directly related to the area inside each of the load-deformation hysteretic loops. This results from the combined effects of contact friction and sliding/gliding motion between the wall and base, and the amount of contact length at the wall-base interface. Fig. 11(a) shows the trailing end of the wall and close inspection shows the wall remained in full contact with the base at peak response and during each of the three tests. Contact at the wall-base interface is further discussed in Section 4.2.

4.2. Wall base response: DIC deformations

To further validate the results from this research, a digital image correlation (DIC) system, as illustrated in Fig. 12 was employed for capturing images and obtain full field displacement measurements at the base of the wall. Fig. 12(a) shows a typical DIC image and Fig. 12(b) depicts the position of the DIC camera system in relation to the test unit. Both of these figures outline the random speckle pattern that was optimized to ensure a speckle quality and size distribution at the wall base necessary for post processing of the DIC images.

The following discussion presents the base displacement analysis at '*Facet Point 1*', see Fig. 12(a), which was subsequently used in calculating the system drift angle based on: Fig. 8(b)

$$\theta_w = \frac{\Delta_T - \Delta_B}{H + h} \text{Pendulum Response}, \tag{5}$$

In the equation above Δ_T and Δ_B are the displacement at the top of the wall and the DIC calculated bottom displacement at the facet *point*, and H and h are shown in Fig. 1(b) and Fig. 8(c). Fig. 13(a) shows the displacement at 'Facet Point 1′, respectively, versus the data point number (i.e., Stage Number) obtained from DIC images. A typical digital image pattern for unit *PT30P* is depicted in Fig. 13(b).

Assuming the wall glides without uplift along its wall-base interface, the horizontal deflection measured by the DIC system (Δ_B) corresponds very well to the measured top wall displacement (Δ_T) considering a pendulum response based on the following calculation:

(a) Near Trailing Wall Toes (b) Along Wall-Base Interface

Fig. 11. Typical Peak Response of Tests.

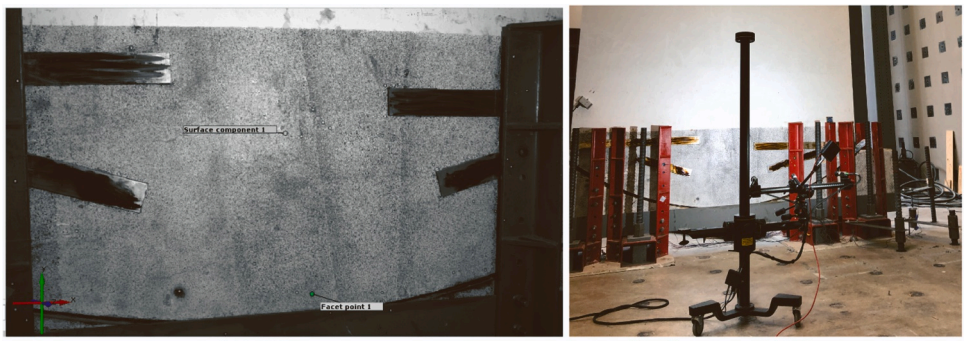

(a) DIC Image (b) Close-up of DIC System

Fig. 12. DIC Image and System and Speckle Pattern.

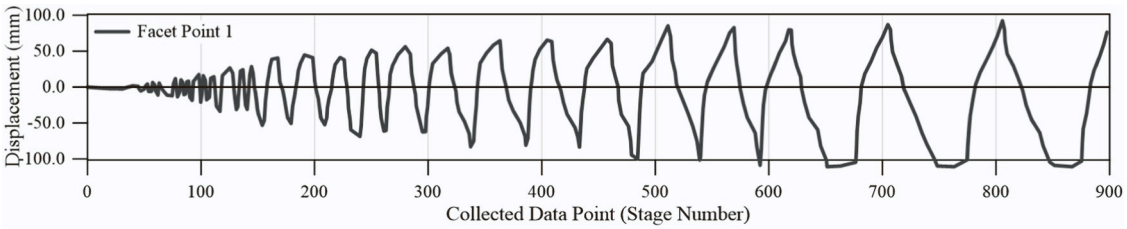

(a) Displacement Facet Point 1 near Base of Wall versus Stage Number

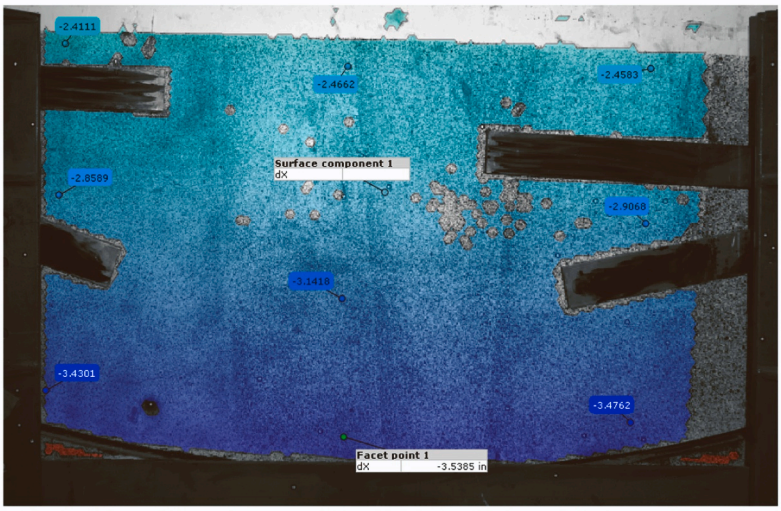

(b) Position of Facet Points and Corresponding Value at Maximum Response

Fig. 13. DIC Base Deformation: Test Unit *PT30P*.

$$\Delta_B = -\Delta_T\left(\frac{R}{H+h-R}\right) \quad (6)$$

At the peak top deflection of $\Delta_T = \pm 101$ mm, see Fig. 8, the base of the wall glides in the opposite direction and the bottom deflection per Eq. (6) is calculated at $\Delta_B = \pm 90$ mm. In the push direction (i.e., positive in Δ_T), the base of the wall glides in the reversed direction (i.e., negative in Δ_B) and the DIC peak bottom deflection is calculated at −115 mm. In the opposite direction (i.e., positive in Δ_B), the DIC peak bottom deflection is + 92 mm, which is much closer to the calculated deflection per Eq. (6). As such, within a degree of confidence it was possible to calculate the system drift based on Eq. (5) and using the wall DIC displacement measurements as depicted in Fig. 13. Results of this analysis are presented in Fig. 14. Once again, the load-drift angle response in Fig. 14, clearly indicates substantial energy dissipation capacity of the test units, drift angles clearly exceeding the required drift angle of 1.78 %, and the wall predominant mode of response was gliding without any significant separation at the wall-base interface.

4.3. Prestress load-deformation response

As previously shown in Fig. 1(b), four unbonded 15 mm diameter post-tensioning (PT) steel threaded bars were used to apply the PT forces. Forces in the PT bars were recorded using low clearance hollow core load cells placed through the threaded bars and installed at each end. Forces in the PT bars provide the main mechanism for the wall to recover its initial configuration and are essential for the wall's lateral load resistance through contact friction. As shown in Fig. 15, during reversed cyclic loading only a slight increase is observed in the PT forces, which is in direct contrast to previous research results on rocking UPTS systems [6,17,53,38,44]. These small deviations in PT force is of significant value to the design of UPTS walls, because ACI ITG-5.1 [2] requires that these systems be subjected to a sequence of displacement-controlled cycles to drift angles in the range of 0.90 % to 3 %. Experimental results on rocking UPTS walls, which are dominated by significant gap opening (i.e., uplift), have shown that yielding

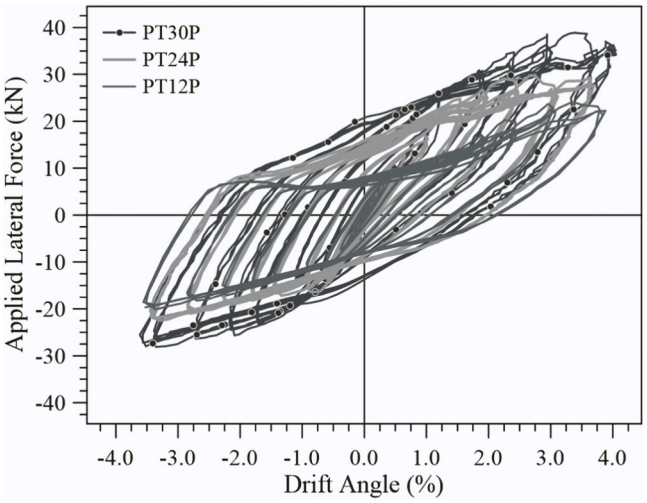

Fig. 14. Lateral Load-Drift Angle Response.

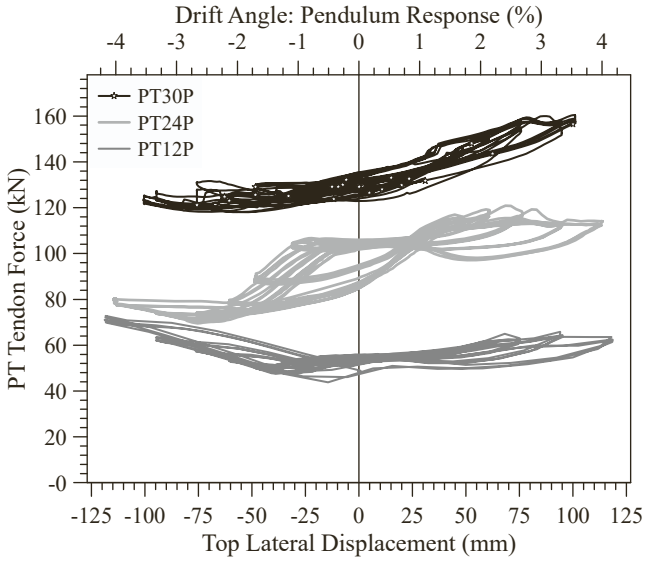

Fig. 15. Prestress Load-Deformation Response.

occurs when the drift angle is close to 1 % [32,44]. Although the drift angle based on Eq. (4) at peak response is around 4–5 %, no signs of yielding of the PT bars were observed in these tests. Previous research has clearly shown that yielding of the PT threaded bars or bars will result in the reduction of PT forces [48], and adversely affect the friction transfer across wall interfaces (ACI ITG-5.2 [3]).

4.4. Strain gage profile response

Strain gage profiles in the push and pull directions are depicted in Fig. 16. This figure only shows data for test unit *PT30P* but this response was also typical in the other two test units. The data shows no signs of strain concentrations along the wall-base interface, and the peak strain at the base of the wall was below 400 micro strains. This strain level is significantly below the level that may cause bearing failure parallel to the direction of the wood grain (~6000 micro strains) [5]. It is clear that the absence of strain concentrations along the wall base results from the test units' pendulum response, which is directly associated to the amount of contact length at the wall-base interface and the strain profile. This behavior can have significant advantages in lateral load resisting systems since the reduction of compression and impact stresses at the wall toes will likely ensure the wall remains damage-free in these regions.

4.5. System lateral performance evaluation

In this research, energy dissipation during load reversal is mainly accomplished with the gliding motion along the wall-base circular path and the interface contact friction. The experimental results previously described substantiate a gliding motion took place with no separation at the wall-base interface and there was significant energy dissipation in the system response. In the next two sections, the system performance is characterized based on the energy dissipation capacity and equivalent damping ratio in each load-deformation cycle.

4.5.1. Dissipated energy in UPTS wall systems

Results in Fig. 17(a) clearly indicate that increasing the PT force also increases the energy dissipation capacity of the system. However, the increase in energy dissipation from unit *PT24P* to unit *PT30P* was negligible. In contrast, for test units *PT24P* and *PT30P* the peak energy dissipation increased by nearly 30 % with respect to test unit *PT12P*. Furthermore and for each test unit, it is clear that under repeated cycles at the same drift angle, there was no significant reduction in the energy dissipation capacity. This clearly shows that the system is capable of maintaining its performance under reversed cyclic loading with

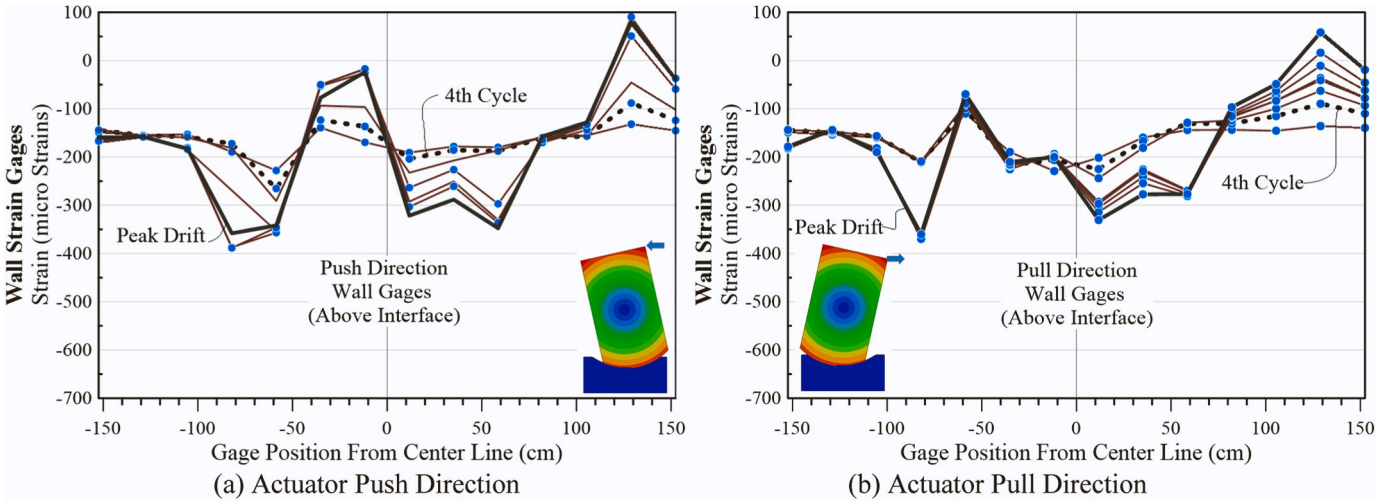

Fig. 16. Strain Gage Profiles: Test Unit *PT30P*.

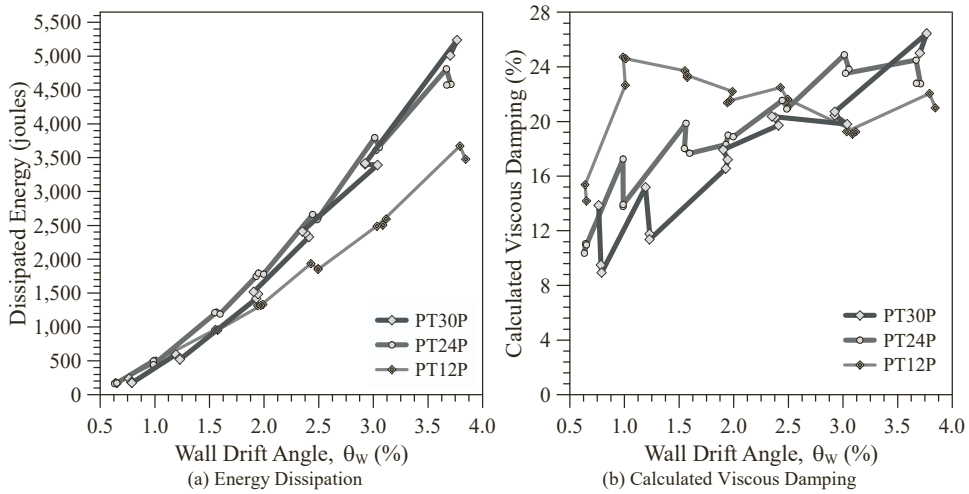

Fig. 17. System Performance Evaluation.

minimum to no damage.

4.5.2. *Equivalent viscous damping ratio*

A physical measure that is of primary significance in seismic design applications, is the equivalent viscous damping (EVD) ratio [40]. Subsequently, the EVD ratio is necessary in calculating the damping reduction factor at peak drift angles [15,21]. The EVD ratio, ξ_{eq}, was computed at each cycle using the following expression [14,26].

$$\xi_{eq} = \frac{1}{4\pi}\frac{E_D}{E_S} \tag{7}$$

In Eq. (7) the EVD ratio is obtained by calculating E_D and E_S, which are the energy dissipation and the recoverable elastic strain energy within each loading cycle outlined in detail in Lu and Silva [33] and others [14,26]. In quasi-static reversed cyclic load tests Eq. (7) is generally a satisfactory approximation for calculating the EVD ratio. This indicates that the inherent elastic damping ratio of 5 % was not included in the analysis.

Using Eq. (7), the EVD ratio can be expressed as a function of the top lateral displacement or drift angle. Referring to Fig. 17(b), the EVD ratio for test units *PT12P*, *PT24P*, and *PT30P* was estimated at 24.7 %, 24.9 %, and 26.5 %, respectively. These results substantiate that at peak response, in any of the three PT levels, the energy dissipation capacity of the system was comparable to the amount of EVD that develops from the hysteretic behavior of conventional reinforced concrete frame members [40]; but significantly higher than currently used LiF systems [8,53] or RC-precast rocking systems [6,31,32]. Research by Dinehart and Blasetti [16], and others have reported energy dissipation values that are significantly smaller that the values depicted in Fig. 17(a). For instance, Dinehart and Blasetti [16] have reported energy dissipation values of 500–3000 joules or nearly 10–50 % of the values reported in Fig. 17(a). Research by Krzan et al. [29] have estimated the equivalent damping ratio and reported values for light framed wood shear walls in the range of 5–30 %, but these values were reported at significant damage levels with significant drop in the registered lateral load under subsequent loading cycles. Using the reported values by Krzan et al., at the peak lateral load, the reported equivalent damping ratios drop to 5–15 % [29]. In comparison, larger amounts of energy dissipation and damping ratios reported in Fig. 17 were not a direct consequence of damage from the structural system, but, through the friction that develops at the wall-base interface. This is a valuable outcome because an increase in the equivalent viscous damping ratio without damage on LFRS, results in an optimum seismic response by decreasing the lateral displacement and force demands in seismic design of LFRS [15,21,39], while achieving the added value to society of achieving a damage-free response.

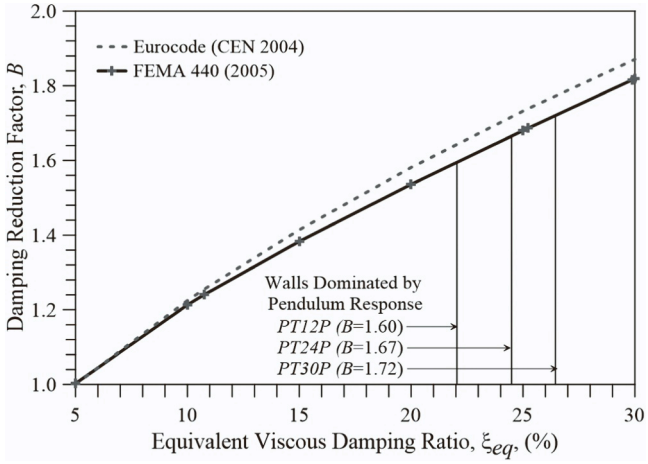

Fig. 18. Damping Reduction Factor.

4.5.3. *Damping reduction factor*

Many design codes and research studies outline design methods based on damping reduction factors [15,21,39]. Damping reduction factors, also termed modification factors, are used in seismic design to modify elastic response spectral values corresponding to a damping ratio of 5 % to other damping levels in terms of the relation:

$$S_a(\xi_{eq}) = \frac{S_a(5\%)}{B} \tag{8}$$

In Eq. (8), $S_a(\xi_{eq})$ is the design spectral acceleration at the target damping ratio or ξ_{eq}, $S_a(5\%)$ is the spectral ordinate obtained at a 5 % damping ratio, and B is the damping reduction factor. As such, B reduces the spectral acceleration from the 5 % damping ratio to the desired ξ_{eq}.

The expressions used to develop the Eurocode [15] and FEMA 440 [21] damping reduction factors are outlined in the work by Cardone et al. [9]. The vertical lines depicted in Fig. 18 correspond to the damping reduction factors calculated for the test units based on the FEMA 440 relations [21], which were obtained according to:

$$B = \frac{4}{5.6 - \ln(\xi_{eq})} \tag{9}$$

In Eq. (9), ξ_{eq} is the EVD ratio obtained per Eq. (7) in units of percent. Table 2 presents a summary of relevant test results at peak response.

Table 2
Summary of Relevant Test Results at Peak Response.

Unit ID	Maximum Displacement, **mm**	**Maximum Drift Angle, (%)**	Maximum Lateral Force, **kN**	Equivalent Viscous **Damping (%)**	Damping Reduction Factor, (*B*)
PT12P	118	3.87	24.42	24.7	1.60
PT24P	119	3.69	30.07	24.9	1.67
PT30P	101	4.05	38.97	26.5	1.72

It is clear the damping reduction factors, *B*, decreased from 1.72 to 1.60, as the post-tensioning force decreased from test unit *PT30P* to *PT12P*. This indicates that increasing the PT force directly led to a reduction of seismic demands by nearly 7.5 %, while increasing the lateral load capacity by nearly 60 %.

5. Conclusions

This paper reported the results of an ongoing research project with the objective of developing a new concept for the construction of unbonded post-tensioned shear (UPTS) walls. Whereas in other UPTS wall systems the wall-base interface is in the form of a flat surface, in the proposed concept this interface is built in a circular profile. The aim of constructing the wall-base interface in the shape of a circular profile is to ensure the wall glides along its base without uplift. Results show that ensuring this gliding motion without uplift is critical in the response of the proposed *pendulum UPTS* walls, and ensures the system dissipates high levels of energy through contract friction while behaving damage-free. Other key findings are summarized as follows:

- The three test units were subjected to increasing drift limits at 4.16 %, 3.98 % and 3.55 % without any signs of damage. These values are higher than the limiting ACI ITG-5.1 acceptance criteria of 3 % drift ratio.
- Ensuring a gliding motion without uplift results in a system that responds in its elastic state, which eliminates the need for extra nailing requirements at the end of wood shear walls or the need of nailing replacement after an earthquake, or extra confinement reinforcement in wall boundaries of RC walls.
- Increasing the applied PT force translated to an increase in the lateral load capacity. For instance, increasing the PT force from 53.4 kN to 133.4 kN, resulted in an increase in the lateral load capacity from 24.42 kN to 38.97 kN, or 43.7 %, which indicates a noticeable effect of the PT force on the lateral load capacity. Likewise, increasing the applied PT force also translated in an increase in the energy dissipation capacity of the system.
- Although no damage was observed or recorded during testing, the estimated peak equivalent viscous damping ratio (EVD) of the three tested walls was 24.7 %, 24.9 %, and 26.5 %, which is comparable to the amount of EVD ratio that develops in conventional reinforced concrete frame members. This is a significant improvement because an increase in the EVD ratio translates in a reduction in the lateral design demands.

Although this paper focuses on a proof of concept for a light frame wood shear wall under increasing levels of post-tensioning force, computational simulations have also shown that many of the promising results observed in this research program can be extrapolated to other systems such as *RC precast pendulum UPTS walls*. Such is the aim of ongoing research on the testing of pendulum UPTS reinforced concrete walls with different circular profiles and subjected to different PT forces.

Finally, preliminary computational analysis has also shown that coupled wall systems comprising of dual *pendulum UPTS* walls can assist in preserving the self-centering capabilities of the system. This condition will be evaluated in future research using nonlinear time history analyses for systems subjected to ground motions.

Declaration of Competing Interest

The authors declare the following financial interests/personal relationships which may be considered as potential competing interests: Pedro F Silva reports financial support was provided by National Science Foundation. If there are other authors, they declare that they have no known competing financial interests or personal relationships that could have appeared to influence the work reported in this paper.

Data availability statement

Some or all data, models, or code generated or used during the study are available from the corresponding author by request.

Acknowledgements

The research presented in this paper is part of a collaborative research project supported by the U.S. National Science Foundation under grant numbers CMMI-1762170 (PI: P.F. Silva) and CMMI-1762119 (PI: R. Burgueño). CNC machining of the Glulam Beams (GLB) and beams used in this research were donated by Sauter Timber LLC. Assistance of Terry Pattillo from WoodWorks – Wood Products Council in securing these donated materials is appreciated. Special thanks to Owen Scholl (High Bay Manager), The GW Machine Shop, and the undergraduate students, Pengyu Chen, Zachary Stecher, Mohammad Badeeb, Florencia Dayan, and Savana Stewart are indeed appreciated.

References

[1] Abaqus (2014), User Manual Version 6.14–2: Dassault systems", Simulia Corp. USA.
[2] ACI Innovation Task Group 5.1 (2007), Acceptance Criteria for Special Unbonded Post-Tensioned Precast Structural Walls Based on Validation Testing and Commentary. ACI ITG-5.1. Farmington Hills, MI ACI.
[3] ACI Innovation Task Group 5.2 (2009), Requirements for Design of a Special Unbonded Post-Tensioned Precast Shear Wall Satisfying ACI ITG-5.1 (ACI ITG-5.2–9) and Commentary. Farmington Hills, MI: ACI.
[4] American Concrete Institute, ACI (2019). ACI 318–19: Building Code Requirements for Structural Concrete and Commentary, American Concrete Institute, Farmington Hills, MI, 624 pp.
[5] American Wood Council (AWC) (2015), "Special Design Provisions for Wind and Seismic (SDPWS), American Wood Council, Leesburg, VA, 97 pp.
[6] Belleri A, Schoettler MJ, Restrepo JI, Fleischman RB. Dynamic behavior of rocking and hybrid cantilever walls in a precast concrete building. ACI Struct J 2014;111 (3):661–72.
[7] Bora C, Oliva MG, Nakaki SD, Becker R. Development of a precast concrete shear-wall system requiring special code acceptance. PCI J 2007;51(1):122–35.
[8] Brown JR, Li M, Palermo A, Pampanin S, Sarti F. Experimental testing of a low-damage post-tensioned C-shaped CLT core-wall. ASCE J Struct Eng 2021;Vol. 147 (No. 3). 16 pp.
[9] Cardone D, Dolce M, Rivelli M. Evaluation of reduction factors for high-damping design response spectra. Bull Earthq Eng 2009;Vol. 7:273–91.
[10] Chalarca B, Bedoya-Ruiz D, Herrera JP. Experimental behavior and seismic performance assessment of unbonded post-tensioned precast concrete walls for low-rise buildings. Eng Struct 2023;Vol. 289:116251.
[11] Chancellor NB, Eatherton MR, Roke DA, Akbaş T. Self-centering seismic lateral force resisting systems: high performance structures for the city of tomorrow. Buildings 2014;4:520–48.
[12] Cheng X, Dong X, Li Y, Lu X, Du X. Experimental study of precast concrete walls with replaceable corner components. Earthq Eng Struct Dyn 2023;Vol. 52(No. 14): 4352–75.
[13] Christovasilis IP, Filiatrault A, Constantinou MC, Wanitkorkul A. Incremental dynamic analysis of wood frame buildings. Earthq Eng Struct Dyn 2009;Vol. 8(No. 4):477–96.

[14] Clough, R.W., and Penzien, J. (2003), Dynamics of Structures, 3rd Edition, Computers & Structures, Inc. 1995 University Ave. Berkeley, CA, 752 pp.
[15] Comité Européen de Normalisation (CEN) (2004), "Eurocode 8: Design of Structures for Earthquake Resistance—Part 1: General Rules, Seismic Actions and Rules for Buildings, EN 1998–1:2004. Brussels, Belgium: CEN, 231 pp.
[16] Dinehart W, Andrew S. Blasetti AS. Comparison of energy dissipation, stiffness, and damage of structural oriented strand board (OSB), conventional gypsum, and viscoelastic gypsum shearwalls subjected to cyclic loads. Buildings 2012;Vol. 2(No. 3):173–202.
[17] Domenico DD, Ricciardi G, Infanti S, Benzoni G. Frictional heating in double curved surface sliders and its effects on the hysteretic behavior: an experimental study. Front Built Environ 2019;Vol. 5(No. 74). 11 pp.
[18] Dorn M, Habrová K, Koubek R, Serrano E. Determination of coefficients of friction for laminated veneer lumber on steel under high pressure loads. Friction 2021;Vol. 9:367–79.
[19] EERI (2010), Chile Earthquake Clearinghouse, The Mw 8.8 Chile Earthquake of February 27, 2010″ EERI Special Earthquake Report, 20 pp. https://www.eeri.org/wp-content/uploads/Van_Turkey_eq-report.pdf and http://eqclearinghouse.org/co/20100227-chile/.
[20] Englekirk RH. Design-construction of the paramount — A 39-story precast prestressed concrete apartment building. PCI J 2002;47(4):56–71.
[21] Federal Emergency Management Agency (FEMA 440) (2005), "Improvement of Nonlinear Static Seismic Analysis Procedures, Prepared by Applied Technology Council (ATC-55 Project) Department of Homeland Security Washington, D.C., 392 pp.
[22] Henry RS, Aaleti S, Sritharan S, Ingham J. Concept and finite-element modeling of new steel shear connectors for self-centering wall systems. J Eng Mech 2010;136(2):220–9.
[23] Holden T, Restrepo JI, Mander JB. Seismic performance of precast reinforced and prestressed concrete walls. ASCE J Struct Eng 2003;129(3):286–96.
[24] Hose YD, Silva PF, Seible F. Performance evaluation of concrete bridge components and systems under simulated seismic loads. EERI Earthq Spectra 2000;16(2):413–42.
[25] Housner GW. The behavior of inverted pendulum structures during earthquakes. Bull Seismol Soc Am 1963;53(2):403–17.
[26] Jacobsen LS. Steady forced vibrations as influenced by damping. ASME Trans 1930;52(1):169–81.
[27] Jafari A, Preti M, Beheshti M, Dugnani R. Self-centering walls strengthening by high-performance concrete: a feasibility study. Mater Struct 2021;Vol. 54(No. 117). 20 pp.
[28] Krawinkler, H., Parisi, F., Ibarra, L., Ayoub, A., and Medina, R. (2001), Development of a Testing Protocol for Wood Frame Structures." CUREE-Caltech Woodframe, Project Rep. No. W-02, Stanford University, Stanford, CA. 99 pp.
[29] Krzan M, Pazlar T, Ber B. Improved seismic response of light-frame-timber panels with cement-particle-board sheathing of various thicknesses and different configurations of fasteners. Eng Struct 2022;Vol. 253(No. 15). 113757-1,14 pp.
[30] Kurama YC. "Seismic design of unbonded post-tensioned precast concrete walls with supplemental viscous damping. Acids Struct J 2000;97(4):641–51.
[31] Kurama YC. Hybrid post-tensioned precast concrete walls for use in seismic regions. PCI J 2002;47(5):36–59.
[32] Kurama YC, Sause R, Pessiki S, Lu LW. Seismic response evaluation of unbonded post-tensioned precast walls. Acids Struct J 2002;99(5):648–58.
[33] Lu B, Silva PF. Estimating equivalent viscous damping ratio for RC members under seismic and blast loadings. Elsevier Int J Mech Res Commun 2006;Vol. 33(No. 6):787–95.
[34] Marriott, D., Pampanin, S., Bull, D., and Palermo, A. (2008), Dynamic Testing of Precast, Post-Tensioned Rocking Wall Systems with Alternative Dissipating Solutions, 2008 Proceedings of the New Zealand Society for Earthquake Engineering Inc., April 2008, Wairakei, New Zealand, Paper No. 39, 16 pp, http://db.nzsee.org.nz/2008/Contents.htm.
[35] Nazari M, Sritharan S, Aaleti S. Single precast concrete rocking walls as earthquake force-resisting elements. Earthq Eng Struct Dyn 2016. https://doi.org/10.1002/eqe.2829.
[36] Ni C, He M, Chen S. Evaluation of racking performance of wood portal frames with different wall configurations and construction details. ASCE J Struct Eng 2012;Vol. 138(No. 8):984–94.
[37] Panian, L., and Bucci, N. (2013), SFPUC Headquarters Building: An Innovative High Performance Structure, STRUCTURE Magazine, April 2013, pp. 30–32.
[38] Perez FJ, Pessiki S, Sause R. Seismic design of unbonded post-tensioned precast concrete walls with vertical joint connectors. PCI J 2004;49(1):58–79.
[39] Priestley MJN. Myths and fallacies in earthquake engineering. Concr Int 1997;Vol. 9(No. 2):54–63.
[40] Priestley MJN, Calvi GM, Kowalsky MJ. Displacement based seismic design of structures. IUSS Press; 2007721 pp..
[41] Priestley MJN, Sritharan S, Conley JR, Pampanin S. Preliminary results and 25 conclusions from the PRESSS five-story precast concrete test building. PCI J 1999;Vol. 44(No. 6):42–67.
[42] Rabinowicz E. The nature of the static and kinetic coefficients of friction. J Appl Phys 1951;Vol. 22(No. 11):1373–9.
[43] Restrepo JI, Rahman A. Seismic performance of self-centering structural walls incorporating energy dissipators. ASCE J Struct Eng 2007;133(11):1560–70.
[44] Schultz, A.E., Erkmen, B., Magaña R.A. (2004) "Seismic Design Factors for Precast Concrete Shear Wall Parking Garages, 13th World Conference on Earthquake Engineering Vancouver, B.C., Canada, Paper no. 2076, 15 pp.
[45] Seo NJ, Armstrong TJ, Drinkaus P. A comparison of two methods of measuring static coefficient of friction at low normal forces: a pilot study. Ergonomics 2009;Vol. 52(No. 1):121–35.
[46] Silva, P.F., Dunne, J., and Burgueño, R. (2020), Self-Centering Pendulum Shear Walls via Nonlinear Elastic Kinematics, Proceeding 17th World Conference on Earthquake Engineering, Paper N° C000733, 11 pp.
[47] Silva, P.F., Lagler, C., Alturki, M., and Burgueño, R. (2022), Nonlinear Dynamic FEM Analysis of Unbonded Posttensioned Coupled Pendulum Shear Walls Linked with Elastic Energy Dissipating Connectors. In Proceedings of the 12th National Conference in Earthquake Engineering.
[48] Smith BJ, Kurama YC, McGinnis MJ. Design and measured behavior of a hybrid precast concrete wall specimen for seismic regions. ASCE J Struct Eng 2011;137(10):1052–62.
[49] Smith BJ, Kurama YC, McGinnis MJ. Behavior of precast concrete shear walls for seismic regions: comparison of hybrid and emulative specimens. ASCE J Struct Eng 2013;139:1917–27.
[50] Stanton, J.F., and Nakaki, S.D. (2002), Design Guidelines for Precast Concrete Seismic Structural Systems, PREcast Seismic Structural Systems (PRESSS), University of Washington (UW) Report No. SM 02–02, Department of Civil Engineering, University of Washington, Seattle, WA, 118 pp.
[51] The Engineered Wood Association, APA (2024), "Diaphragms and Shear Walls Design and Construction Guide, Design and construction recommendations for engineered diaphragm systems in floor, shear wall and roof systems, Form No. 350K/Revised May 2024, 37 pp.
[52] Tiwari S, Dash SR, Mondal G, Roy K. Analysis and design of RC unbonded PT shear walls in isolation and integrated into buildings: a state-of-the-art review. Structures 2023;Vol. 56:104790. 20 pp.
[53] To TX, Dao TN, Aaleti S, van de Lindt JW, Rammer DR. Hybrid system of unbonded post-tensionedCLT panels and light-frame wood shear walls. ASCE J Struct Eng 2017;Vol. 143(No. 2). 12 pp.
[54] Toranzo LA, Restrepo JI, Mander JB, Carr AJ. Shake-table tests of confined-masonry rocking walls with supplementary hysteretic Damping. J Earthq Eng 2009;13(6):882–98.
[55] Yeh B, Williamson T, Keith E. Combined shear and wind uplift resistance of wood structural panel shearwalls. Struct Congr 2009: Don't Mess Struct Eng 2009:1662–72.